Contributed Papers from Materials Science and Technology 2017 (MS&T17)
October 8 – 12, 2017, David L. Lawrence Convention Center, Pittsburgh, Pennsylvania USA

DOI 10.7449/2017/MST_2017_1045_1053

HOT ROLLING EFFECT UPON THE HIGH TEMPERATURE JOHNSON-COOK STRENGTH AND FAILURE MODELS FOR A 15V38 GRADE STEEL

M.F. Buchely[1*], D.C. Van Aken[1], R.J. O'Malley[1], S. Lekakh[1], K. Chandrashekhara[2]

[1] Department of Materials Science and Engineering. Missouri University of S&T, Rolla, MO, 65401, USA.
[2] Department of Mechanical and Aerospace Engineering. Missouri University of S&T, Rolla, MO, 65401, USA.

Keywords: Finite-Element simulation, Hot metal rolling, Johnson-Cook model, Mechanical characterization.

Abstract

High temperature failure tests of a commercially produced 15V38 grade steel (0.37% C, 1.37% Mn, 0.56% Si, 0.13% Cr, 0.09% V) were studied in the cast and hot-rolled condition to deliver a material model. Mechanical testing was performed using a hydraulic load frame adapted to perform tensile tests at different temperatures (up to 1300^oC) and different strain-rates (up to 20 s^{-1}). Plastic flow behavior and the strain at failure of the steel were approximated using the Johnson-Cook Strength and the Johnson-Cook Failure models. Hot-rolled material shows more consistent strength and failure data as compared to the as-cast material. The experimental coefficients of these material models were implemented in ANSYS-AUTODYN FEM to replicate the tensile experiments. The accuracy of each test curve was determined by comparing the experimental data with the simulated results. It was found that FEM simulation with these two Johnson-Cook models predicts well the deformation behavior of the tested steel during the tensile load at studied range of strain-rates and temperatures. These models can be implemented to simulate thermomechanical deformation during hot rolling to predict possible defects.

Introduction

Approximately 80% of all metal products undergo hot working during some part of their processing history [1]. One of the main hot working operations is hot rolling, which is characterized by non-isothermal, large deformations at high strain rates (10^{-3} to 10^3 s^{-1}) and high temperatures (above 900^oC) [2, 3].

Due to the recent improvements in numerical modeling techniques, such as Finite Element Modelling (FEM), hot rolling can now be better understood. FEM has permitted significant reductions in the cost and time of both the design and the analysis of hot rolling operations. The numerical simulations have been done to determine an optimal hot rolling schedules before any actual trial runs [4-7]. Application of these modeling techniques requires suitable and accurate constitutive equations for metal behavior in the hot working regimes. However, due the complexity of the problem, suggested universal models cannot handle correctly a large variety of important for practice variables. A specific steel and the hot rolling parameters needed to be investigated to obtain an accurate material model available to predict material behaviors during hot rolling [8].

One model commonly used to model plasticity of metals at different strain-rates and temperatures is the Johnson-Cook (JC) strength model [9]. JC constitute equation relates the effective stress (σ_{eff}) as a function of the plastic strains (ε_{pl}), plastic strain-rates ($\dot{\varepsilon}_{pl}$) and temperatures (T), as follows:

* Corresponding Author: e-mail: buchelym@mst.edu

$$\sigma_{eff} = \left(A + B\varepsilon_{pl}^{n}\right)\left(1 + C\ln\frac{\dot{\varepsilon}_{pl}}{\dot{\varepsilon}_0}\right)\left(1 - \left(\frac{T - T_r}{T_m - T_r}\right)^{m}\right) \quad (1)$$

where *A, B, C, n, m* are material parameters; $\dot{\varepsilon}_0$ is a strain-rate of reference, T_r is a reference temperature, and T_m is the melting temperature [10].

Because this JC strength model does not predicts material failure, modeling the macro mechanical damage in the material needs an additional failure model. One failure model available in many commercial FE software is the Johnson-Cook failure model [11], which relates the strain at failure of the material (ε^f) to the triaxiality stresses ($\sigma^* = \sigma_{hydrostatic} / \sigma_{eff}$), plastic strain-rates ($\dot{\varepsilon}_{pl}$), and temperatures (T), as follows:

$$\varepsilon^f = \left(D_1 + D_2 \exp\frac{\sigma_{hydrostatic}}{\sigma_{eff}}\right)\left(1 + D_4 \ln\frac{\dot{\varepsilon}_{pl}}{\dot{\varepsilon}_0}\right)\left(1 - D_5\frac{T - T_r}{T_m - T_r}\right) \quad (2)$$

Parameters D_1 to D_5 must be experimentally determined using a test that involves failure of the material, e.g. tensile test. Damage (D) during FE analysis is defined as follows:

$$D = \sum \frac{\Delta\varepsilon}{\varepsilon^f} \quad (3)$$

where ($\Delta\varepsilon$) is the change of plastic strain which occurs during an integration cycle [11].

In this paper, commercially produced 15V38 grade steel was studied in its "as-cast" and "hot-rolled" conditions. The objective was to characterize the properties of this steel at typical range of strain-rates and temperatures used in industry.

Materials and Methods

Commercial grade 15V38 grade steel was received in the "as-cast" condition, as a 9" diameter x 1' long round bar. Chemical composition of this steel is shown in Table I. Material was sectioned in 1.5" square bars, and this squares bars were austenitized at 950ºC for one hour and hot-rolled to 0.71" diameter round bars (approx. 82% reduction) using an instrumented Rolling Mill (STANAG TA-315). Tensile specimens were machined from both conditions: "as-cast" and "hot-rolled' in a CNC lathe (Haas model LT-1). Different geometry shapes were manufactured, as shown in Figure 1(a). Metallographic specimens of the as-cast and hot-rolled steel were prepared in accordance with ASTM E3-11.

Mechanical testing was performed using a MTS hydraulic load frame specifically adapted to perform high temperature tensile tests at different strain-rates. Figure 1(b) shows a schematic view of this system, which consist of pulling bars, LVDT device to measure the displacement, and a furnace (up to 1400°C) around the testing area. Actual tests were performed between 900^oC and 1100^oC temperatures, and between 0.001 s^{-1} (quasi-static Q.S.) and 20 s^{-1} strain rates. Argon gas was flowing during the test to reduce oxidation in the specimen. Engineering stress (σ_{eng}) - strain (e) curves were transformed to true stress (σ_{true}) – true strain (ε) curves using the following relations [2]:

$$\varepsilon = \ln(1 + e), \quad \text{and} \quad \sigma_{true} = \sigma_{eng}(1 + e) \quad (4)$$

The final area of the specimen at the failure surface was measured using a digital microscope (Dino-Lite Edge) and the strain at failure (ε^f) was calculated as follows [2]:

$$\varepsilon^f = \ln(A_0 / A_f) \quad (5)$$

where A_0 and A_f are the initial and final area of the specimen, respectively.

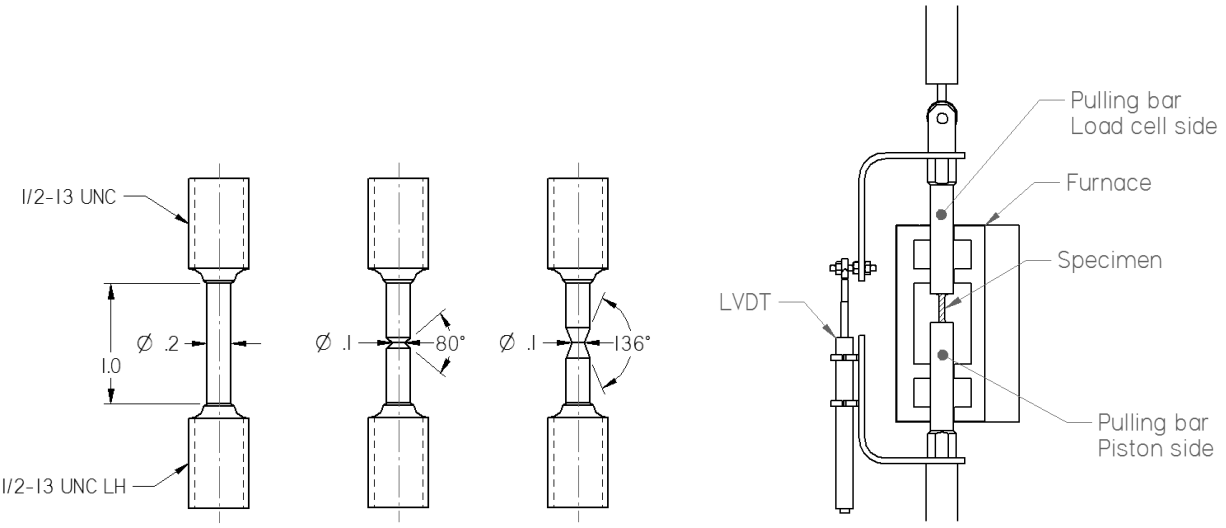

(a) (b)

Figure 1. Methodology of hot tensile tests: (a). three specimen geometries: (smooth round, notch 1 and notch 2), (b) schematic view of the system tensile system.

Table I. Chemical composition: 15V38 grade steel (wt.%)

C	Mn	P	S	Si	Ni	Cr	Mo	Cu	Al	V
0.37	1.37	0.011	0.055	0.56	0.06	0.13	0.01	0.14	0.006	0.091

Table II. Physical, elastic, and thermal properties for FE simulation of 15V38 grade steel.

Density [kg/m^3]	Specific heat [$J/kg.K$]	Elastic modulus [GPa]	Poisson's ration
7900	200	210	0.29

True stress-true strain data was adjusted to the JC strength model (eq.(1)). To calibrate the JC parameters, a Genetic-Algorithm optimization process was programmed in MATLAB toolbox [12]. In this optimization process, the strain-rate of reference ($\dot{\varepsilon}_0$) was included as material parameter, according to the analysis suggested by Schwer [13].

FE simulations of the tensile test were performed using these JC parameters, in order to find the state of triaxiality (see Eq.(2)) during tensile test. The FE analysis was modeled as a 2D axis-symmetrical model in the explicit code ANSYS/AUTODYN. An additional physical, elastic and thermal properties needed for simulation for this steel were assumed to be constant, and they are shown in Table III. During the simulations, the state of hydrostatic stress, effective stress and effective plastic strain were tracked for the central node in the necking area. Using this information, the JC failure model (Eq.(2)) was adjusted. Parameters were calibrated by a nonlinear-least-squares curve fitting method and followed a procedure explained by Corona and Orient [14].

After that, FE simulations including both JC strength model and JC failure model were performed, and final experimental and computational load-displacement curves were compared.

Results and Discussion

Microstructures of studied material in "as-cast" and "hot-rolled" conditions are shown in the Figure 2. Non-metallic inclusions and macropores were observed in the "as-cast" material before etching (Figure 2(a)). The etched microstructure (Figure 2(b)) revealed proeutectoid ferrite (light contrast) and pearlite

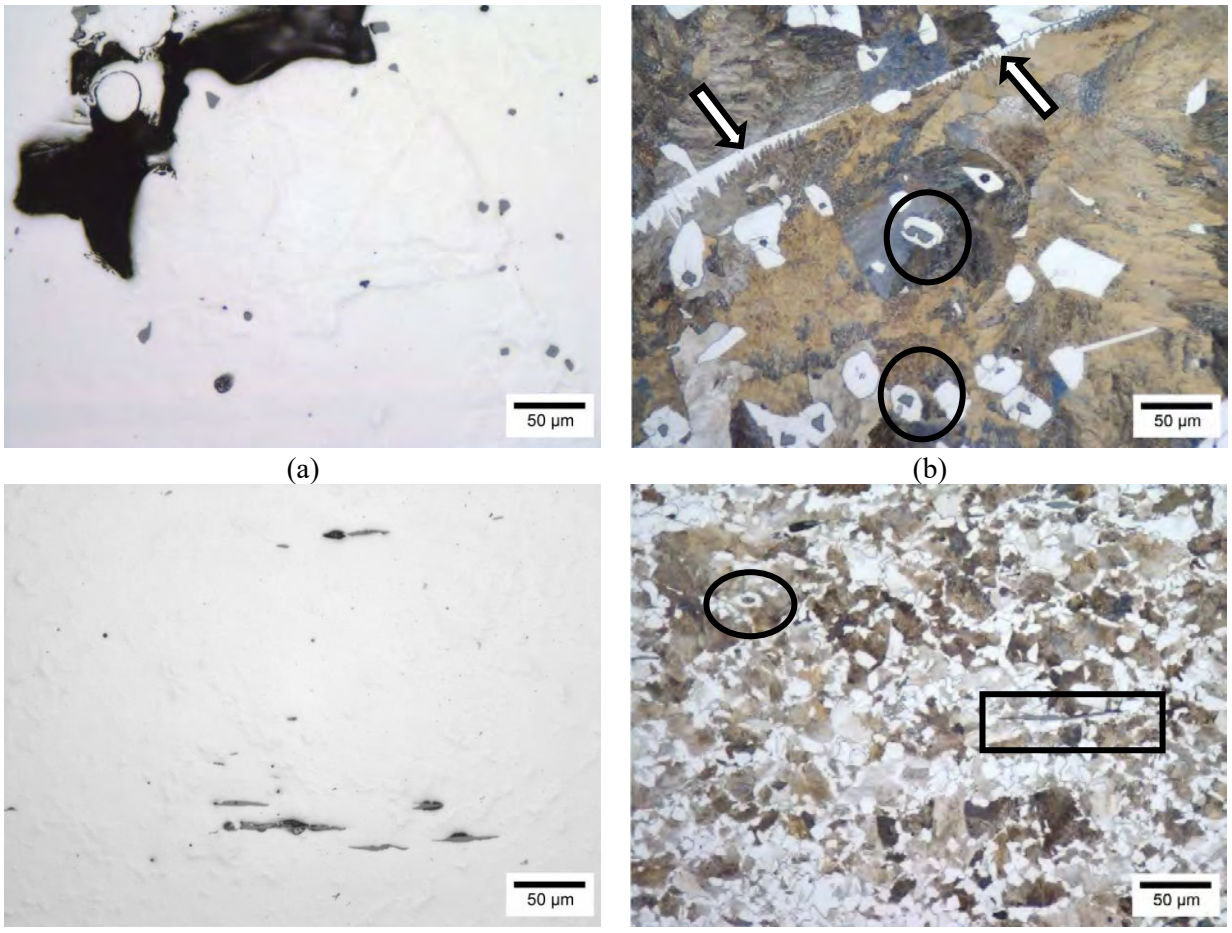

(a) (b)

(c) (d)

Figure 2. Microstructures of the 15V38 grade steel at two conditions: "as-cast", (a) polished and (b) etched; and "hot-rolled" (c) polished and (d) etched. Images (c) and (d) were taking in the rolling direction.

(dark contrast). Ferrite grains were nucleated at two preferred sites: grain-boundaries (arrows) and Type III MnS inclusions (circles). A large prior-austenite grain can be estimated following the ferrite along the grain boundaries. Figure 2(b) shows part of this boundary (arrows), and, the grain size was on the order of 1mm. Microstructure of the "hot-rolled' material before etching (Figure 2(c)) shows the MnS inclusions as stringers parallel to the rolling direction, and pores appear to be smaller. According to Wang *et* al. [15], a 50% reduction at 900ºC and 1200ºC is sufficiently to closure micro-pores during hot rolling. Therefore, considering the 82% reduction used in the current study, it was expected to have a decrease of porosity after hot rolling. A more homogenous distribution of the allotriomorphic ferrite (light contrast) and pearlite (dark contrast) is shown in the (Figure 2(d)). A MnS inclusion parallel to the rolling direction is also shown (squares). Some of the ferrite is heterogeneously nucleating at the MnS inclusions (circle). Prior-austenite grain size was measured at higher magnification (not shown), by following the proeutectoid ferrite along the prior austenite grain boundaries. The average grain size for the hot rolled steel was 20μm.

Stress-strain curves, both engineering and true, are shown in Figure 3 for the "as-cast" and "hot-rolled" conditions. In general, each material exhibits higher stress at higher strain-rates and lower temperatures.

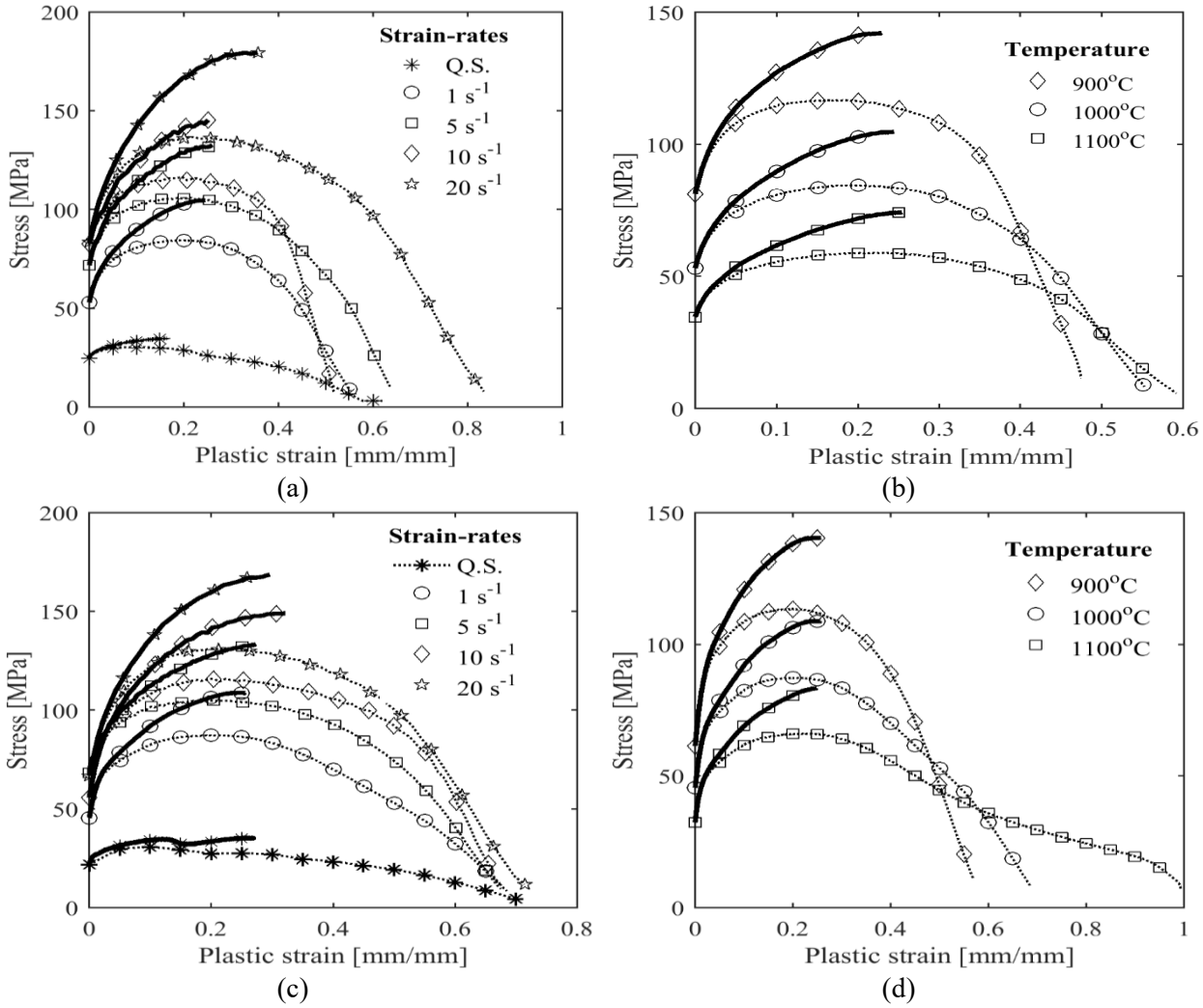

Figure 3. Stress-Plastic strain curves at different test conditions: (a) and (b) as-cast, and (c) and (d) hot-rolled 15V38 steel. Figures (a) and (c) at $1000^{o}C$; and (b) and (d) at 1 s^{-1} strain-rate. Q.S.: Quasi-static test at 0.001 s^{-1}. Solid lines: true stress – true strain curves, and dot lines: engineering stress – engineering strain.

Additionally, the ductility of materials tends to decrease at lower temperatures. Calculated from engineered data, true strain and true strain (Eq.(4)) were only applied to the "stable" part of the curve, which is generally limited by the maximum load during test or before a visible necking begins to form in the specimen. After the test, specimens were cleaned, and pictures of the final shape were taken in both directions (Figure 4(a)). The fracture surface was used to measure the final area and the strain at failure and used in Eq.(5) to calculate strain at failure (Table III).

Table IV shows the JC parameters that were calibrated by Genetic-Algorithm optimization process using the true stress – true strain data. Figure 5(a) shows the comparison between the measured plastic stress and the predicted ones by JC model. A good agreement was achieved using the calibrated JC parameters. According to these results, it can be noticed that the plastic behavior for both material conditions (as cast and hot rolled) are similar in the range of tested strain-rates and temperatures (see Figure 3 and Table III).

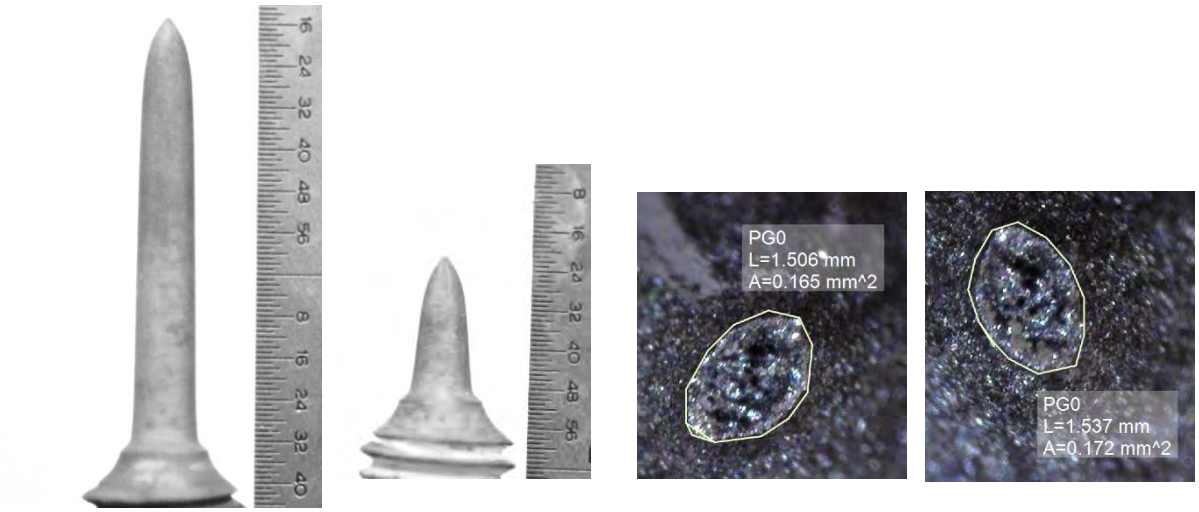

(a) (b)

Figure 4. Hot-rolled specimen after 1000^oC and 10 s^{-1} tensile test: (a) shape profile showing two halves of failed specimen, and (b) fracture surface in both halves. The average fracture area was calculated from parts.

Table III. Summary of mechanical behavior for the 15V38 at different test conditions.

	Yield stress [*MPa*]		Max. true stress [*MPa*]		Strain at failure	
test	"as-cast"	"hot-rolled"	"as-cast"	"hot-rolled"	"as-cast"	"hot-rolled"
Q.S.*, 1000^oC	24.9	22.9	35.1	34.7	3.84	4.99
1 s^{-1}, 1000^oC	53.1	45.6	104.9	109.0	3.99	4.99
5 s^{-1}, 1000^oC	71.9	68.4	132.7	133.5	4.05	4.92
10 s^{-1}, 1000^oC	82.7	55.8	145.5	149.2	3.30	4.98
20 s^{-1}, 1000^oC	83.6	66.9	179.6	168.8	3.68	4.34
1 s^{-1}, 900^oC	83.6	61.5	142.3	140.7	2.94	4.57
1 s^{-1}, 1100^oC	34.6	32.4	74.2	83.5	4.93	5.45
Notch 1, 1 s^{-1}, 1000^oC	-	-	156.4	177.4	1.21	2.53
Notch 2, 1 s^{-1}, 1000^oC	-	-	153.6	168.9	2.08	2.92

*Q.S. Quasi-static test: 0.001 s-1.

Table IV. Calibrated JC strength model parameters by tensile experimental data: 15V38 grade steel.

	A [MPa]	B [MPa]	n	C	m	$\dot{\varepsilon}_0$ [s^{-1}]	T_r [^oC]
"as-cast"	16.9428	45.9149	0.5554	0.6224	0.6394	0.0299	1000
"hot-rolled"	12.9564	65.8189	0.3373	0.3452	0.7814	0.0299	1000

The elongation and strain at failure significantly changed between these two conditions, and the hot rolled steel has larger elongation to failure (Figure 5(b)). It can be noticed that the elongation at failure randomly scattered at different strain-rates for the "as-cast" condition, while it was more consistent for the "hot-rolled" condition. This increase in strain at failure after preliminary hot rolling is related to several microstructural changes: (i) homogenizes the microstructure, (ii) reduced grain size, and (iii) reduce the porosity.

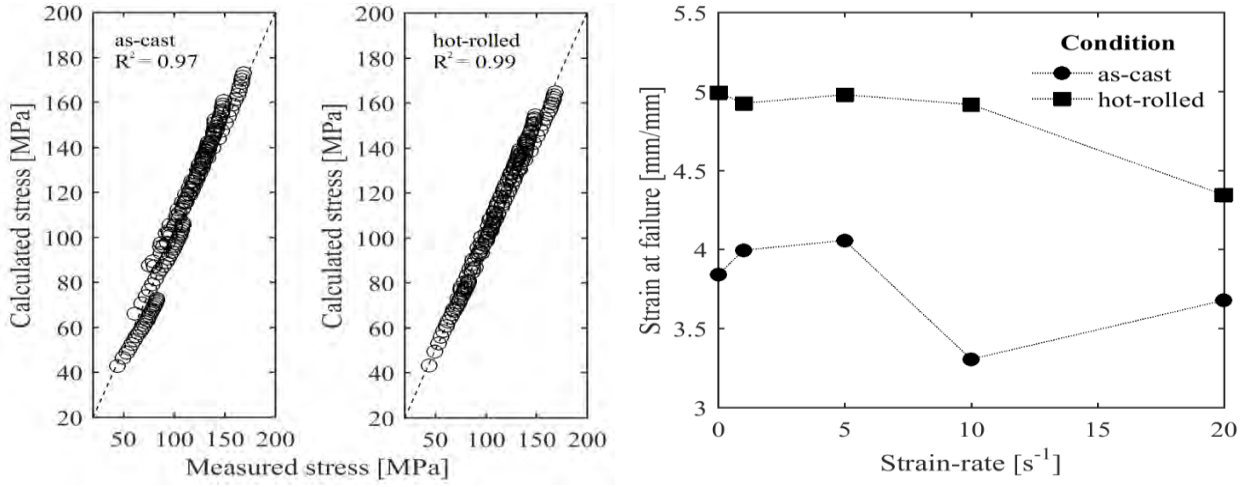

(a) (b)

Figure 5. (a) Comparison between experimental plastic stresses and predicted stresses by JC model, using parameters found by Genetic-Algorithm optimization process (see Table IV), and (b) strain at failure comparison at different strain-rates.

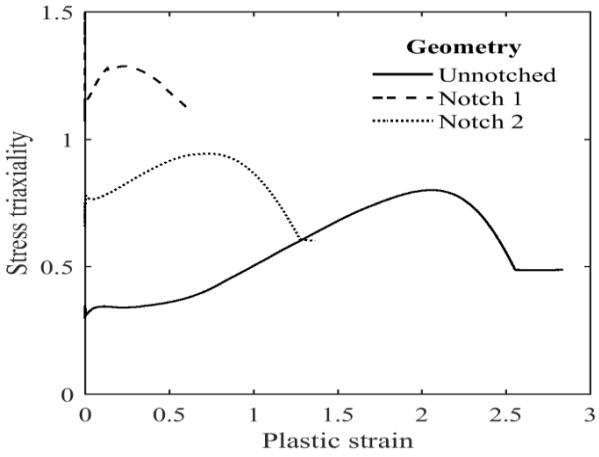

Figure 6. Simulated change in stress triaxiality during the tensile test in the center of the three specimen geometries shown in Figure 1(a) for the "as-cast" condition, 1 s^{-1} strain rate, and 1000 ℃, and (b) comparison of simulated and experimental specimen profiles.

Figure 6(a) shows the simulated change of stress triaxiality during the tensile test for the three different studied geometries. The stress triaxiality increased during the initial part of tensile test due to the formation of the neck in the specimen until a maximum point. After this point, triaxiality tends to reduce due to the large deformations reached at high temperatures. From the triaxiality results and experimental strain at failure at different test conditions (Table III), the JC failure model parameters were calibrated, and they are shown in Table V.

To verify precision of both JC models (strength and failure), the experimentally obtained coefficients were implemented in FEM model and full simulation of tensile test was performed. Figure 7(a) shows the results of this analysis. Notice that maximum damage ($D = 1$) is reached at the neck area, where the failure of the material occurs. This figure also shows a comparison between the experimental and predicted final profile of the specimen. Figure 7(b) shows final experimental and computational load-displacement curve. Good agreement was achieved using the FE analysis.

Table V. Calibrated JC failure model parameters for 15V38 grade steel.

Condition	D_1	D_2	D_3	D_4	D_5	$\dot{\varepsilon}_0$ [s^{-1}]	T_r [^oC]
"As-cast"	0.025	12.502	-2.2101	-0.059	1.45	1	1000
"Hot-rolled"	0.041	1.075	-0.7341	-0.038	1.29	1	1000

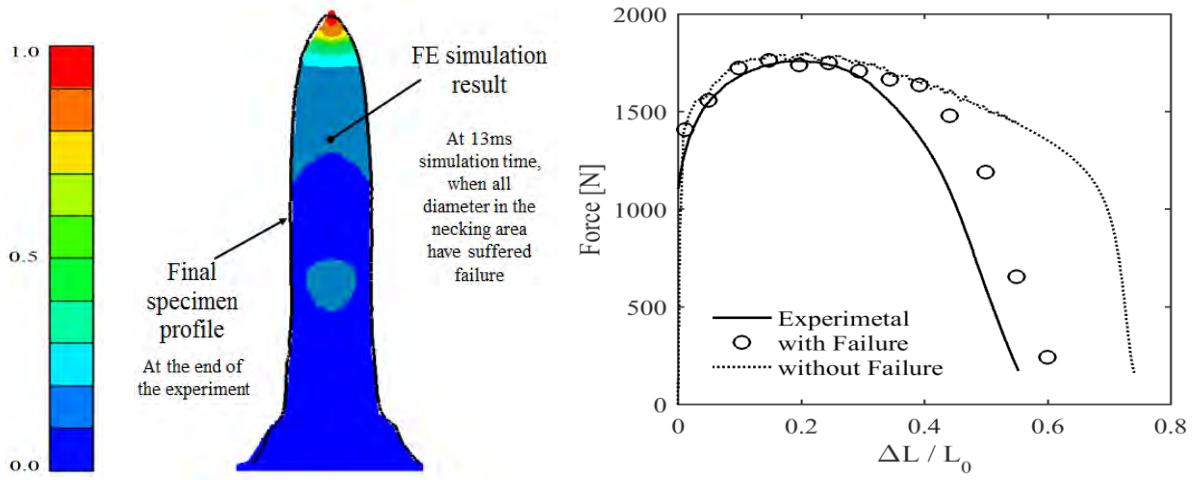

(a) (b)

Figure 7. Simulation results: (a) Comparison of simulated and experimental specimen profiles, and (b) final experimental and computational load-displacement curve.

Conclusions

The commercially produced 15V38 grade steel was studied in its "as-cast" and "hot-rolled" conditions. The high temperature mechanical properties and failure were characterized at the range of temperature and strain rates typical for industrial hot rolling conditions. The two JC strength and JC failure models parameters were delivered from experiment and calibrated. Hot-rolled process generates more homogeneous and less porous microstructure, which is related to a more consistent strength and failure data than the as-cast material. FE simulations shows good agreement between experimental and predicted final profile of the specimen using calibrated parameters.

Acknowledgements

This work is supported by the Peaslee Steel Manufacturing Research Center at Missouri University of Science and Technology. The investigators acknowledge to the next companies for financial support: Gerdau, Nucor, SSAB and US Steel.

References

1. Brown, S.B., K.H. Kim, and A. L., *An internal variable constitutive model for hot-working of metals.* International Journal of Plasticity, 1989. **5**: p. 95-130.
2. Dieter, G., *Mechanical Metallurgy*. 1986: McGraw-Hill.
3. Hosford, W.F. and R.M. Caddell, *Metal forming: mechanics and metallurgy*. 2011: Cambridge University Press.
4. Suehiro, M., et al., *Computer modeling of microstructural change and strength of low carbon steel in hot strip rolling.* Transactions of the Iron and Steel Institute of Japan, 1987. **27**(6): p. 439-445.
5. Beynon, J.H. and C.M. Sellars, *Modelling microstructure and its effects during multipass hot rolling.* ISIJ international, 1992. **32**(3): p. 359-367.
6. Davenport, S., et al., *Development of constitutive equations for modelling of hot rolling.* Materials Science and Technology, 2000. **16**(5): p. 539-546.

7. Wang, X., et al., *Modeling of mass flow behavior of hot rolled low alloy steel based on combined Johnson-Cook and Zerilli-Armstrong model.* Journal of Materials Science, 2017. **52**(5): p. 2800-2815.
8. Banerjee, A., et al., *Determination of Johnson cook material and failure model constants and numerical modelling of Charpy impact test of armour steel.* Materials Science and Engineering A, 2015. **640**: p. 200-209.
9. Gambirasio, L. and E. Rizzi, *On the calibration strategies of the Johnson-Cook strength model: Discussion and applications to experimental data.* Materials Science and Engineering A, 2014. **610**: p. 370-413.
10. Johnson, G.R. and W.H. Cook, *A constitutive model and data for metals subjected to large strains, high strain rates and high temperatures*, in *7th International Symposium on Ballistics (1983)*. 1983. p. 541-547.
11. Johnson, G.R. and W.H. Cook, *Fracture characteristic of three metals subjected to various strains, strain rates, temperatures and pressures.* Engineering Fracture Mechanics, 1985. **21**: p. 31-48.
12. Matlab, *Global Optimization Toolbox, User's Guide*. 2015, MatWorks INC.
13. Schwer, L. *Optional Strain-Rate Forms for the Johnson Cook Constitutive Model and the Role of the Parameter Epsilon_0*. in *6th European LS-DYNA Conference*. 2007.
14. Corona, E. and G. Orient, *An evaluation of the Johnson-Cook model to simulate puncture of 7075 aluminum plates.* 2014, Sandia National Laboratories, SAND2014-1550.
15. Wang, A., P. Thomson, and P. Hodgson, *A study of pore closure and welding in hot rolling process.* Journal of Materials Processing Technology, 1996. **60**(1-4): p. 95-102.